LS Note No. 200

April, 1992

Effect of Eddy Current in the Laminations on the Magnet Field

Y. Chung and J. Galayda

Advanced Photon Source

Argonne National Laboratory

Argonne, IL 60439

Abstract

In this note theory and measurements of the effect of the eddy current in the laminations on the magnet field will be presented. The theory assumes a simple solenoid–type magnet with laminated iron core and ignores the end field effect. The measurements were made on the input voltage and current, and the dipole component of the magnetic field in the middle of the magnet bore. The amplitude and phase relations between these quantities give the field attenuation factor, the phase delay, and the resistance and inductance of the magnet as functions of frequency. Comparisons of the results with the theory will be discussed.

1. Introduction

The proposed corrector magnets to be used for global and local orbit corrections in the storage ring have six poles like sextupole magnets, and in response to the beam motion, a current of up to approximately 50 Hz will be applied varying with time. The corresponding time–varying magnet field in the iron core induces an eddy current in the magnet laminations, which not only decreases the field strength but also produces power loss due to ohmic heating.

The eddy current effect can be reduced significantly by using thin laminations for the iron core. The current design thickness of the lamination is 0.025”. From the viewpoint of curbing the eddy current effect, the thinner the laminations, the better. However, the larger number of thinner laminations required to assemble a magnet of given length will drive up the cost of magnet manufacturing.

This study investigates the effectiveness of the current design for the sextupole/corrector magnet in terms of the attenuation and phase shift of the magnet field and the power efficiency.

2. Impedance of Electromagnetic Fields

For time–varying electromagnetic fields with harmonic time dependence $e^{-i\omega t}$ in conductors and ferromagnetic materials, the complex field impedance Z can be obtained from consideration of Poynting’s theorem for harmonic time variation of the fields,[1]

$$\frac{1}{2}\int_V \mathbf{J}^* \cdot \mathbf{E}\ d^3x - \int_V \left(E \cdot \frac{\partial \mathbf{D}^*}{\partial t} - \mathbf{H}^* \cdot \frac{\partial \mathbf{B}}{\partial t} \right)_{av} d^3x + \oint_S \mathbf{S} \cdot \mathbf{n}\ da = 0, \qquad (2.1)$$

where **n** is the unit vector outward normal to the surface and **S** is the complex Poynting vector defined by

$$\mathbf{S} = \frac{1}{2}\mathbf{E} \times \mathbf{H}^*. \qquad (2.2)$$

In Eq. (2.1) the quantities **E**, **H**, and **J** are assumed to change with time as $e^{-i\omega t}$, while the magnetic flux **B** satisfies only the periodicity condition

$$\mathbf{B}(t + T) = \mathbf{B}(t) \ . \tag{2.3}$$

T (= $2\pi/\omega$) is one period of oscillation and $(\cdots)_{av}$ means time–averaging over T, that is,

$$(\cdots)_{av} = \frac{1}{2T}\int_0^T (\cdots)\ dt \ . \tag{2.4}$$

Consider a two–terminal passive electromagnetic system as in Fig. 2.1, e.g., an electromagnet, connected to an external power supply with output voltage V_i and current I_i.

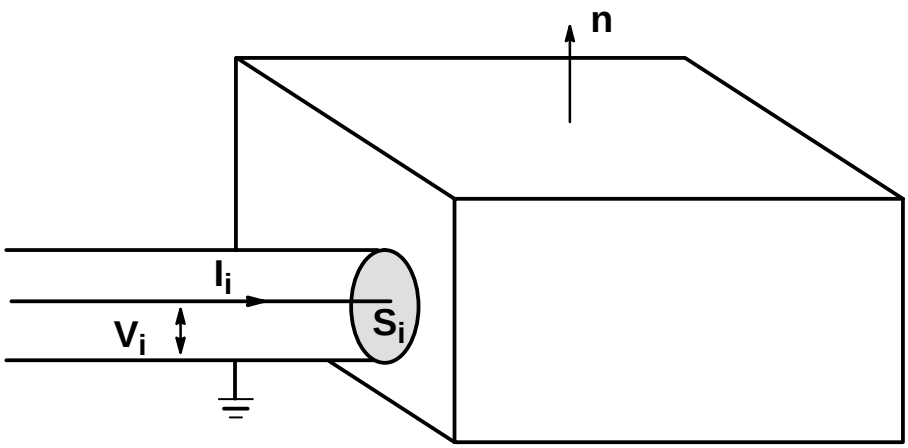

Fig. 2.1: A schematic of a two–terminal passive electromagnetic system.

In Fig. 2.1, the volume V of the system is the rectangular box and the surface of integral S is its surface. The surface integral in Eq. (2.1) can be divided into

$$\oint_S \mathbf{S}\cdot\mathbf{n}\ da = \int_{S_i} \mathbf{S}\cdot\mathbf{n}\ da + \int_{S-S_i} \mathbf{S}\cdot\mathbf{n}\ da \ . \tag{2.5}$$

The first term in Eq. (2.4) is the complex input power

$$\int_{S_i} \mathbf{S}\cdot\mathbf{n}\ da = -\frac{1}{2} I_i^* V_i \ . \tag{2.6}$$

Since the electric energy density is negligibly small compared to the magnetic energy density in ferromagnetic material, we drop the displacement current term in Eq. (2.1). From Eqs. (2.1), (2.5), and (2.6), we obtain

$$\frac{1}{2} I_i^* V_i = \frac{1}{2}\int_V \mathbf{J}^*\cdot\mathbf{E}\ d^3x + \int_V \left(\mathbf{H}^*\cdot\frac{\partial \mathbf{B}}{\partial t}\right)_{av} d^3x + \int_{S-S_i} \mathbf{S}\cdot\mathbf{n}\ da \ . \tag{2.7}$$

Equation (2.6) is the relation between the input power and the various sources of power consumption, whose real part gives the conservation of energy for the time–averaged quantities and whose imaginary part relates to the reactive or stored energy and its alternating flow. Let $Z_i = R - i\omega L$ be the input impedance of a purely inductive system. Then from

$$V_i = I_i Z_i = I_i (R - i\omega L) \tag{2.8}$$

and Eq. (2.7), we obtain

$$R = \frac{1}{|I_i|^2}\left\{\int_V \mathbf{J}^* \cdot \mathbf{E}\ d^3x + 2\mathrm{Re}\int_V \left(\mathbf{H}^* \cdot \frac{\partial \mathbf{B}}{\partial t}\right)_{av} d^3x + 2\int_{S-S_i} \mathbf{S}\cdot\mathbf{n}\ da\right\}, \tag{2.9}$$

and

$$L = -\frac{2}{\omega|I_i|^2}\left\{\mathrm{Im}\int_V \left(\mathbf{H}^* \cdot \frac{\partial \mathbf{B}}{\partial t}\right)_{av} d^3x\right\}. \tag{2.10}$$

Here, we assumed that the conductivity and the radiation loss through $S - S_i$ are real.

Equations (2.9) and (2.10) are the expressions for the resistance and the reactance of a passive electromagnetic system. The power loss, or dissipation, is expressed by the resistance in Eq. (2.9). For an electromagnet, the first term is the loss by Joule heating in the coil winding and the iron core, the second term is the hysteretic loss, and the third term is the radiated power. In the following sections, we will discuss power loss due to the hysteresis effect and the eddy current in the magnet lamination.

3. Hysteresis Effect

Suppose the driving magnetic field **H** has harmonic time dependence $e^{-i\omega t}$ with an amplitude of H_1. Then, in an isotropic ferromagnetic material, the magnetic flux **B** can be written as

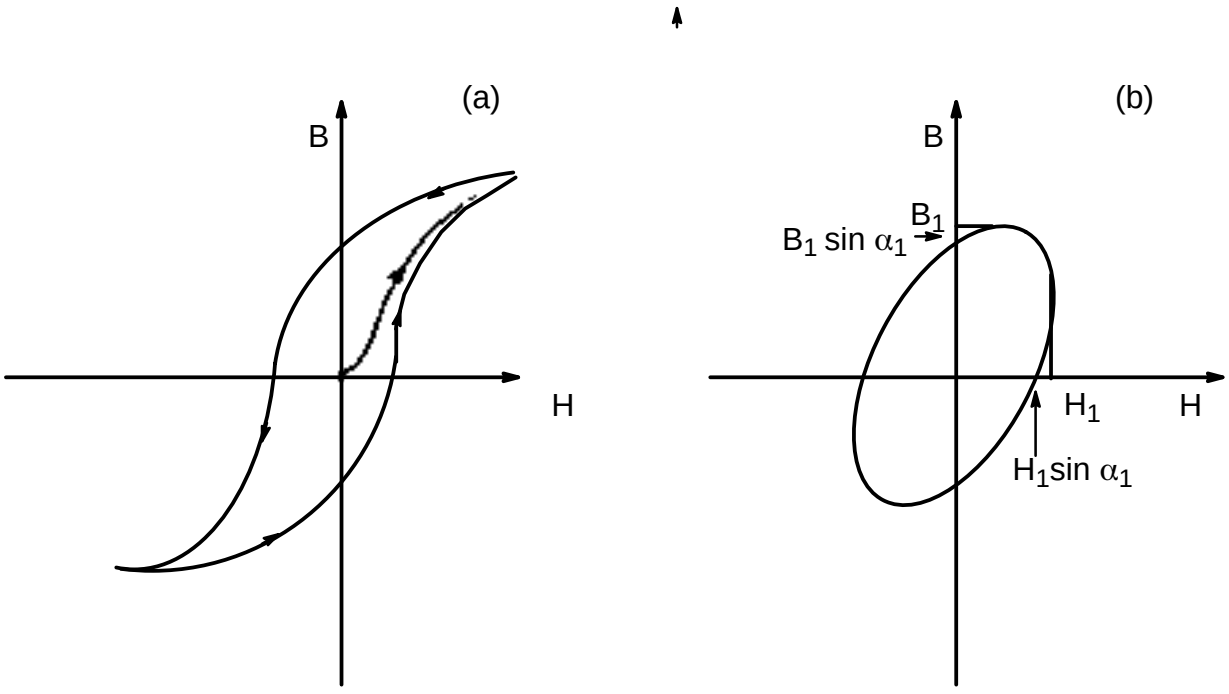

Fig. 3.1: (a) Hysteresis loop giving B in a ferromagnetic material as a function of H. (b) The first harmonic component of the B–H curve in (a).

$$\mathbf{B}(t) = \mathbf{h} \sum_{n=-\infty}^{\infty} B_n e^{-i(n\omega t - \alpha_n)} . \tag{3.1}$$

h is a unit vector in the direction of the magnetic field **H**, and α_n is the phase delay of the n–th harmonic with respect to **H**. We now assume that the conductivity σ is real and that the radiation loss is negligible. Then the resistance R can be written as, from Eqs. (2.8) and (3.1),

$$R = \frac{1}{|I_i|^2} \int_V \frac{1}{\sigma} |\mathbf{J}|^2 d^3x + \frac{\omega}{|I_i|^2} \int_V \sin\alpha_1 H_1 B_1 d^3x . \tag{3.2}$$

where we used

$$\frac{1}{T} \int_0^T e^{i\omega(1-n)t}\, dt = \delta_{n,1} . \tag{3.3}$$

As shown in Eq. (3.2), all other harmonic terms other than n = 1 vanish, and when α_1 is greater than 0, there is a net loss of power proportional to the area enclosed by the ellipse in Fig. 3.1(b).

Another effect of the hysteresis is the reduction of the magnet inductance, as can be seen from Eq. (2.9). When the conductivity σ is real, and if the load is purely inductive (X = ωL), the magnet inductance L is, from Eq. (2.10)

$$L = \frac{1}{|I_i|^2} \int_V \cos\alpha_1 H_1 B_1 d^3x. \tag{3.4}$$

Equations (3.2) and (3.4) show that the hysteresis effect and the eddy current effect cannot be separated. In general, the phase delay α_1 is a function of the field amplitude H_1 as well as of the space, and the field amplitude H_1 (and B_1 also) is in turn affected by the eddy current in the conductor. In the following section, we will derive the eddy current distribution in the magnet lamination and the field attenuation as functions of the lamination thickness and the skin depth.

4. Eddy Current Effect

In this section, we will consider the effect of the eddy current in the magnet lamination on the magnet field and the resulting change in the resistance R and the inductance L. With finite conductivity of the magnet iron, time–varying current applied on the coil winding will produce an eddy current in the core in the direction canceling the original magnetic field. This results in the decrease of the magnet field efficiency and the phase shift of the field with respect to the current in the coil winding.

In order to reduce this undesirable effect and also for the convenience of manufacturing, a magnet core is made of many thin laminations, which are electrically insulated from each other. Since the current flux line must close on itself, the eddy current circulates confined within a lamination and does not cross over to adjacent ones. In the limit of infinitely thin laminations, the current flux lines cancel each other macroscopically and there is no eddy current effect.

Because of the finite conductivity of the magnet iron, eddy currents produce Joule heating and increase the resistance. Reduction of the magnetic field decreases the magnet induc-

tance. This can be shown as follows. Let us for the moment ignore the effect of the hysteresis ($\alpha_1 \to 0$) and focus on the effect of the eddy current with real conductivity σ. We also assume that the magnet is purely inductive. In this case, using the notation of Section 3, Eqs. (2.8) and (2.9) reduce to

$$R = \frac{1}{|I_i|^2} \int_V \frac{1}{\sigma} |\mathbf{J}|^2 d^3x \,, \tag{4.1}$$

and

$$L = \frac{1}{|I_i|^2} \int_V H_1 B_1 d^3x \,. \tag{4.2}$$

Equation (4.1) shows that the resistance of a magnet is the overall power loss due to Joule heating divided by the square of the input current amplitude. The Joule heating occurs primarily in the coil winding and in the magnet lamination. If the resistance change of the coil winding over the frequency range of interest is negligibly small, the dominant source of resistance change with frequency is the eddy current in the magnet lamination. Another effect of the eddy current in the lamination is reduction of the magnet inductance due to the partial cancellation of the magnetic field as shown in Eq. (4.2).

In the following, we will derive the current distribution **J** and the field **H** inside the magnet lamination of finite thickness. The distribution of the eddy current in the laminations and the resulting field in the magnet bore will be obtained as functions of the lamination thickness and the skin depth.

4.1. Distribution of the Eddy Current and the Field in the Lamination

Consider a simple magnet with M laminations of thickness d, with coil wound around it. Let N be the number of windings and $I = I_i\, e^{-i\omega t}$ be the current in the coil. L_x, L_y, and L_z are dimensions along x, y, and z, respectively. The schematic of the magnet is shown in Fig. 4.1. The magnet volume V_m occupied by the laminations is then

$$V_m = MdL_yL_z \,. \tag{4.3}$$

Ignoring the displacement current $\partial\mathbf{D}/\partial t$ and assuming $\varepsilon = \varepsilon_0$, we have

$$\mathbf{J} = \nabla \times \mathbf{H} \quad \text{and} \quad \mathbf{H} = -\,i\frac{1}{\mu\omega\sigma}\nabla \times \mathbf{J} \,, \tag{4.4}$$

where we used $\mathbf{J} = \sigma\mathbf{E}$. Since the current flux lines cannot cut across the boundary between laminations, there will be a circulating current contained inside the narrow lamination. Now, we can imagine two opposing current fluxes of the same magnitude flowing through the gap between adjacent laminations, so that there is a circulating current around each lamination. If we assume the relative permeability K_m ($= \mu/\mu_0$) to be very large, the effect of the this imaginary circulating current on other laminations will be negligible, since all the field lines will be nearly perpendicular to the magnet surface.

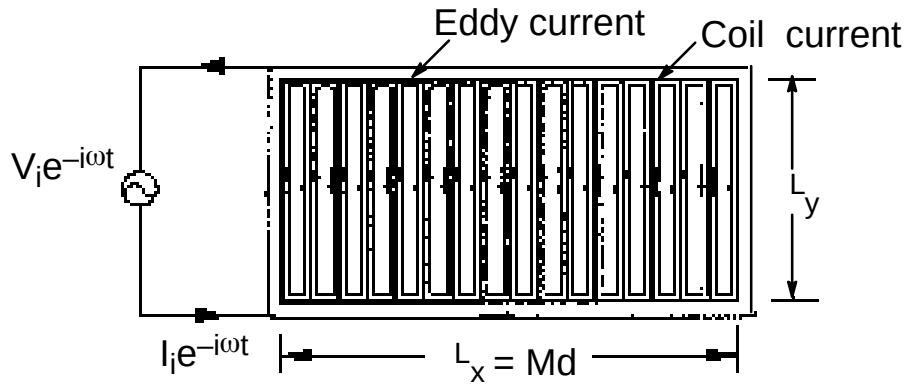

Fig. 4.1: Eddy current in the magnet lamination due to time–varying current.

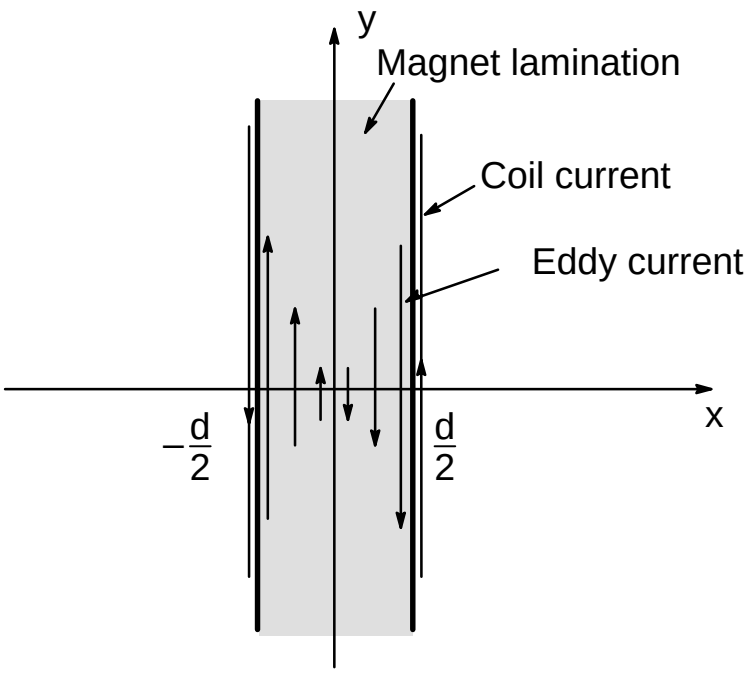

Fig. 4.2: Distribution of the eddy current in the magnet lamination. $J_y(x = 0) = 0$ and there is an infinitely thin current surrounding the lamination.

In Fig. 4.2, the lamination has thickness d, and there is current flowing in the –y direction at x = –d/2 and in the +y direction at x = d/2. Then, from Eq. (4.4), the equation for the current flux J_y in the lamination is

$$\nabla^2 J_y + k^2 J_y + k^2 \frac{NI_i}{L_z}\left\{\delta\left(x-\frac{d}{2}\right)-\delta\left(x+\frac{d}{2}\right)\right\} = 0\,, \tag{4.5}$$

where

$$k^2 = i\mu\omega\sigma = \frac{2i}{\delta^2}\,. \tag{4.6}$$

$\delta\left(=\sqrt{2/\mu\omega\sigma}\right)$ is the skin depth and k is the complex wave number. Since the lamination thickness d is much smaller than L_y and L_z, we can put

$$\frac{\partial}{\partial y} = \frac{\partial}{\partial z} = 0\,. \tag{4.7}$$

With $\nabla^2 = \frac{d^2}{dx^2}$ in Eq. (4.5), the solution is

$$J_y = \frac{k}{\cos\,(kd/2)}\,\frac{NI_i}{L_z}\,\sin\,(kx)\,, \tag{4.8}$$

and the field distribution is, from Eq. (4.4),

$$\begin{aligned} \mathbf{H} &= H_z\hat{z}\,, \\ H_z &= \frac{NI_i}{L_z}\,\frac{\cos\,(kx)}{\cos\,(kd/2)}\,. \end{aligned} \tag{4.9}$$

4.2. Field Attenuation due to the Eddy Current

Equation (4.9) indicates that the magnetic field is reduced from the nominal value NI_i/L_z at x = d/2 due to the eddy current. To get the field at distances near the magnet pole in the air, we average Eq. (4.9) with respect to x. Then, from the continuity condition that B_z be continuous across the boundary between the lamination and the air, we multiply it by μ/μ_0. Therefore,

$$H_z^a = \frac{\mu}{\mu_0}\,\frac{NI_i}{L_z}\,\frac{2}{kd}\,\tan\!\left(\frac{kd}{2}\right). \tag{4.10}$$

From Eq. (4.10) we obtain the field attenuation factor

$$\frac{2}{kd}\,\tan\!\left(\frac{kd}{2}\right) = a(\Delta)\;e^{-i\varphi(\Delta)}\,, \tag{4.11}$$

where

$$a(\Delta) = \frac{\sqrt{2}}{\Delta}\sqrt{\frac{\tan^2(\Delta/2) + \tanh^2(\Delta/2)}{1 + \tan^2(\Delta/2)\,\tanh^2(\Delta/2)}}, \tag{4.12}$$

and

$$\varphi(\Delta) = \frac{\pi}{4} - \tan^{-1}\!\left(\frac{\tanh(\Delta/2)}{\tan(\Delta/2)}\right) - \tan^{-1}(\tanh(\Delta/2)\,\tan(\Delta/2)), \tag{4.13}$$

with $\Delta = \frac{d}{\delta} = d\sqrt{\frac{\mu\omega\sigma}{2}}$. When Δ is very small a(Δ) and φ(Δ) can be approximated as

$$a(\Delta) \approx 1 - \frac{7}{360}\Delta^4 = 1 - \frac{7}{1440}d^4(\mu\omega\sigma)^2, \qquad (\Delta << 1) \tag{4.14}$$

and

$$\varphi(\Delta) \approx -\frac{1}{6}\Delta^2 = -\frac{1}{12}d^2\mu\omega\sigma. \qquad (\Delta << 1) \tag{4.15}$$

Table 4.1 lists values of a(Δ) and φ(Δ) in cases of 0.025” and 0.0625” laminations at 25 Hz, 60 Hz and 200 Hz. The plots for a(Δ) and φ(Δ) are shown in Fig. 4.3. The conductivity of σ = $2.17\times10^6\ \Omega^{-1}m^{-1}$ is assumed.

Table 4.1: Attenuation and phase shift due to the eddy current in the magnet lamination. Three cases of K_m (500, 1000 and 5000) at frequencies 25 Hz, 60 Hz, and 200 Hz with lamination thickness d = 0.025” and d = 0.0625” are given. $\sigma = 2.17\times10^6\ \Omega^{-1}m^{-1}$ is assumed.

K_m = 500		d = 0.025” = 0.635 mm			d = 0.0625” = 1.59 mm		
f (Hz)	δ (mm)	Δ	a(Δ)	φ(Δ) (°)	Δ	a(Δ)	φ(Δ)(°)
25	3.056	0.207	1.000	–0.41	0.519	0.999	–2.58
60	1.973	0.321	1.000	–0.99	0.804	0.992	–6.16
200	1.080	0.586	0.998	–3.29	1.468	0.920	–19.3

K_m = 1000		d = 0.025” = 0.635 mm			d = 0.0625” = 1.59 mm		
f (Hz)	δ (mm)	Δ	a(Δ)	φ(Δ) (°)	Δ	a(Δ)	φ(Δ)(°)
25	2.161	0.293	1.000	–0.82	0.734	0.994	–5.15
60	1.395	0.454	0.999	–1.98	1.137	0.969	–12.1
200	0.764	0.829	0.991	–6.55	2.076	0.767	–32.5

K_m = 5000		d = 0.025” = 0.635 mm			d = 0.0625” = 1.59 mm		
f (Hz)	δ (mm)	Δ	a(Δ)	φ(Δ) (°)	Δ	a(Δ)	φ(Δ)(°)
25	0.966	0.656	0.996	–4.11	1.642	0.884	–23.2
60	0.624	1.016	0.980	–9.73	2.543	0.632	–40.0
200	0.342	1.854	0.830	–28.0	4.643	0.304	–46.1

4.3. Impedance Change due to the Eddy Current

Let R_e be the resistance increase per volume due to the eddy current J_y. The magnet resistance R is then the sum of the resistance R_c due to the coil winding and the resistance increase due to the eddy current, which is R_e times V_m (= NdL_yL_z), the volume occupied by the laminations. That is,

$$R = R_c + R_e V_m \, . \tag{4.16}$$

From Eqs. (4.1) and (4.9), we obtain

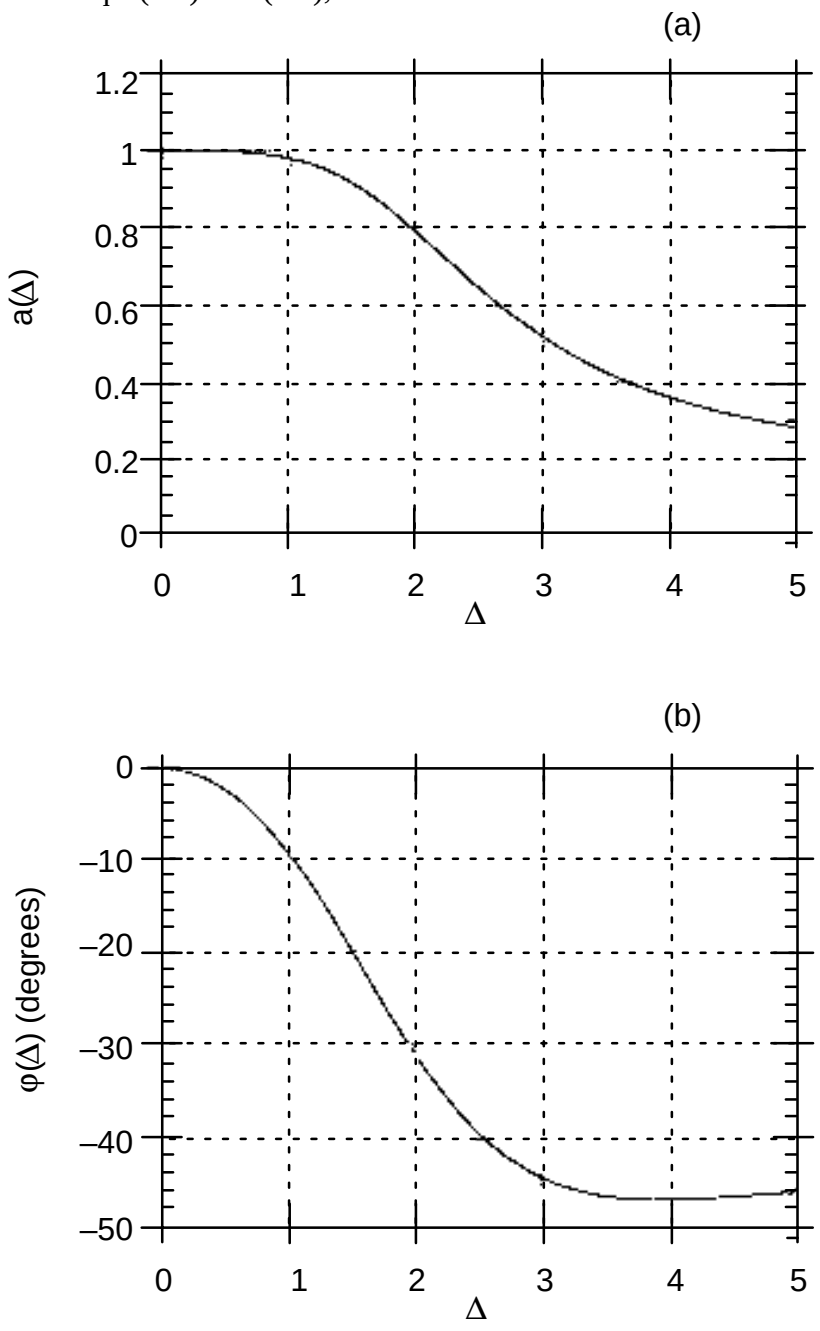

Fig. 4.3: Plotting of (a) the field attenuation factor a(Δ) and (b) the phase shift of the field φ(Δ) with respect to the driving current as functions of $\Delta = \frac{d}{\delta}$.

$$R_e = \frac{1}{\sigma d \left|I_i\right|^2} \int_{-d/2}^{d/2} dx \left|J_y\right|^2$$

$$= \frac{|k|^2}{d \left|\cos(kd/2)\right|^2} \left|\frac{N}{L_z}\right|^2 \int_{-d/2}^{d/2} dx \left|\sin(kx)\right|^2. \tag{4.17}$$

Using the relations

$$\sin(kx) = \sin\left(\frac{1+i}{\delta}x\right) = \sin\left(\frac{x}{\delta}\right)\cosh\left(\frac{x}{\delta}\right) + i\cos\left(\frac{x}{\delta}\right)\sinh\left(\frac{x}{\delta}\right),$$

$$\cos(kx) = \cos\left(\frac{1+i}{\delta}x\right) = \cos\left(\frac{x}{\delta}\right)\cosh\left(\frac{x}{\delta}\right) - i\sin\left(\frac{x}{\delta}\right)\sinh\left(\frac{x}{\delta}\right) \tag{4.18}$$

we obtain

$$R_e = \mu\omega\left|\frac{N}{L_z}\right|^2 r(\Delta), \tag{4.19}$$

where $\Delta = \frac{d}{\delta}$ and

$$r(\Delta) = \frac{\sinh\Delta - \sin\Delta}{\Delta\,(\cosh\Delta + \cos\Delta)}. \tag{4.20}$$

Figure 4.4 (a) shows the plot for r(Δ). When the lamination is much thinner than the skin depth ($\Delta << 1$), we have

$$R_e \approx \frac{\mu\omega}{6}\left|\frac{N}{L_z}\right|^2 \Delta^2 = \frac{1}{12}\left|\frac{N}{L_z}\right|^2 \sigma(\mu\omega d)^2, \qquad (\Delta << 1) \tag{4.21}$$

and in the opposite case ($\Delta >> 1$), we have

$$R_e \approx \mu\omega\left|\frac{N}{L_z}\right|^2 \frac{1}{\Delta} = 2\left|\frac{N}{L_z}\right|^2 \frac{1}{d}\sqrt{\frac{\mu\omega}{2\sigma}}\ . \qquad (\Delta >> 1) \tag{4.22}$$

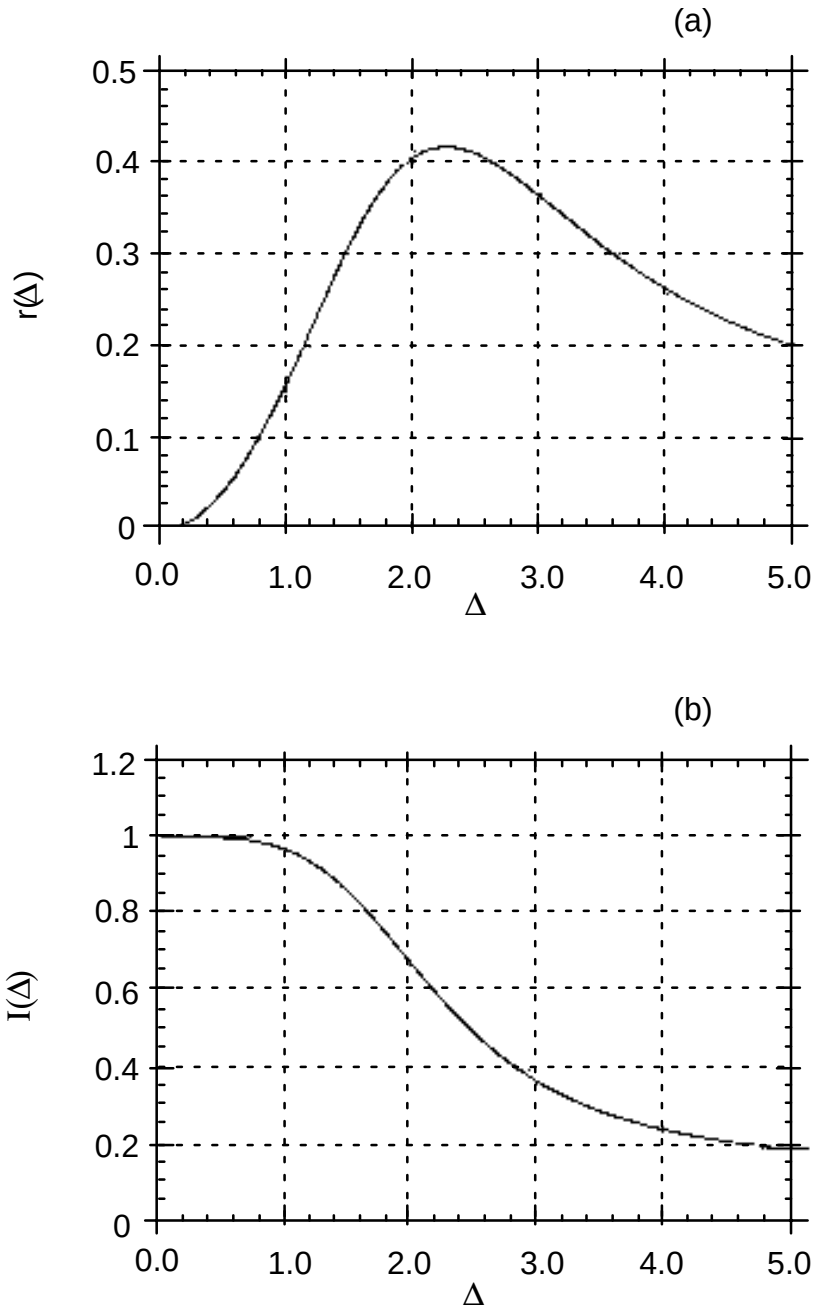

Fig. 4.4: Plotting of the functions: (a) r(Δ) in Eq. (4.19) and (b) l(Δ) in Eq. (4.27).

For a given magnet, the resistance increase due to the eddy current is proportional to the square of frequency when the frequency is low, as shown in Eq. (4.21). However, as the frequency increases further, the resistance increase slows down and in the limit of high frequency it grows only as the square root of the frequency.

To calculate the inductance change due to the eddy current, we should consider the magnetic field not only in the lamination but also in the coil and in the air. The inductance L of a magnet is the total stored magnetic energy divided by half the square of the input current amplitude. That is, from Eq. (3.4) with $\alpha_1 = 0$,

$$L = \frac{1}{\left|I_i\right|^2}\left\{\int_{\text{lamination}} H_1 B_1 d^3x + \int_{\text{air}} H_1 B_1 d^3x\right\}. \tag{4.23}$$

The inductance contribution from the lamination can be obtained in a fashion similar to calculation of the resistance, which gives L_{el}, the average inductance per volume of the lamination. To estimate the magnetic energy stored outside the magnet, we introduce V_{eff}, the effective volume in the air that contains the magnetic flux. Then we can write

$$L = L_{el}V_m + L_{ea}V_{eff}. \tag{4.24}$$

Let us write L_{ea} in terms of H_z^a, the field near the magnet pole as given by Eq. (4.10), as

$$L_{ea} = \frac{\mu_0}{\left|I_i\right|^2}\left|H_z^a\right|^2 = \frac{\mu^2}{\mu_0}\left|\frac{N}{L_z}\right|^2 a(\Delta)^2. \tag{4.25}$$

Then V_{eff} is the total magnetic energy stored in the air divided by $\frac{1}{2}L_{ea}|I_i|^2$. V_{eff} may be estimated roughly by multiplying the length of a magnet and the area of a polygon constructed by connecting adjacent magnet poles.

We now proceed to calculate L_{el}. From Eq. (4.9), we have

$$\begin{aligned} L_{el} &= \frac{\mu}{d\left|I_i\right|^2}\int_{-d/2}^{d/2} dx\left|H_z\right|^2 \\ &= \frac{\mu}{d\ |\cos\ (kd/2)|^2}\ \left|\frac{N}{L_z}\right|^2 \int_{-d/2}^{d/2} dx\ |\cos\ (kx)|^2. \end{aligned} \tag{4.26}$$

Using Eq. (4.18), we obtain

$$L_{el} = \mu\left|\frac{N}{L_z}\right|^2 l(\Delta), \tag{4.27}$$

where $\Delta = \frac{d}{\delta}$ and

$$l(\Delta) = \frac{\sinh\Delta + \sin\Delta}{\Delta\ (\cosh\Delta + \cos\Delta)}. \tag{4.28}$$

The plot for $l(\Delta)$ is shown in Fig. 4.4 (b). When the lamination is much thinner than the skin depth ($\Delta << 1$), we have

$$L_{el} \approx \mu\left|\frac{N}{L_z}\right|^2\left(1 - \frac{1}{30}\Delta^4\right) = \mu\left|\frac{N}{L_z}\right|^2\left\{1 - \frac{d^4}{120}(\mu\omega\sigma)^2\right\}, \qquad (\Delta << 1) \tag{4.29}$$

and in the opposite case ($\Delta >> 1$), we have

$$L_{el} \approx \mu\left|\frac{N}{L_z}\right|^2\frac{1}{\Delta} = \left|\frac{N}{L_z}\right|^2\frac{1}{d}\sqrt{\frac{2\mu}{\omega\sigma}}\ . \qquad (\Delta >> 1) \tag{4.30}$$

From Eqs. (4.26) and (4.30), we have

$$L_{ea}/L_{el} \approx O\left(\frac{\mu}{\mu_0}\right) >> 1 \tag{4.31}$$

and the inductance change due to the eddy current is dominated by the field outside the magnet laminations unless V_{eff} is much smaller than V_m.

5. Measurement of the Eddy Current Effect

In this section, we will discuss measurements of the eddy current effect on a storage ring sextupole magnet with horizontal/vertical correction winding. The measurements were made on the input voltage and current, and the dipole component of the magnetic field in the middle of the magnet bore. The amplitude and phase relations among these quantities give the field attenuation factor $a(\Delta)$, the phase delay $\varphi(\Delta)$ and the resistance and the inductance of the magnet as functions of frequency. Comparisons of the results with the theory discussed in the previous sections will be presented.

5.1 Setup

In Fig. 5.1 is shown the setup for the measurement of the eddy current effect on the magnet field. For this measurement, the correction coil windings on four of the six magnet poles, except the top and bottom poles, were connected in series in vertical correction (horizontal field) configuration.

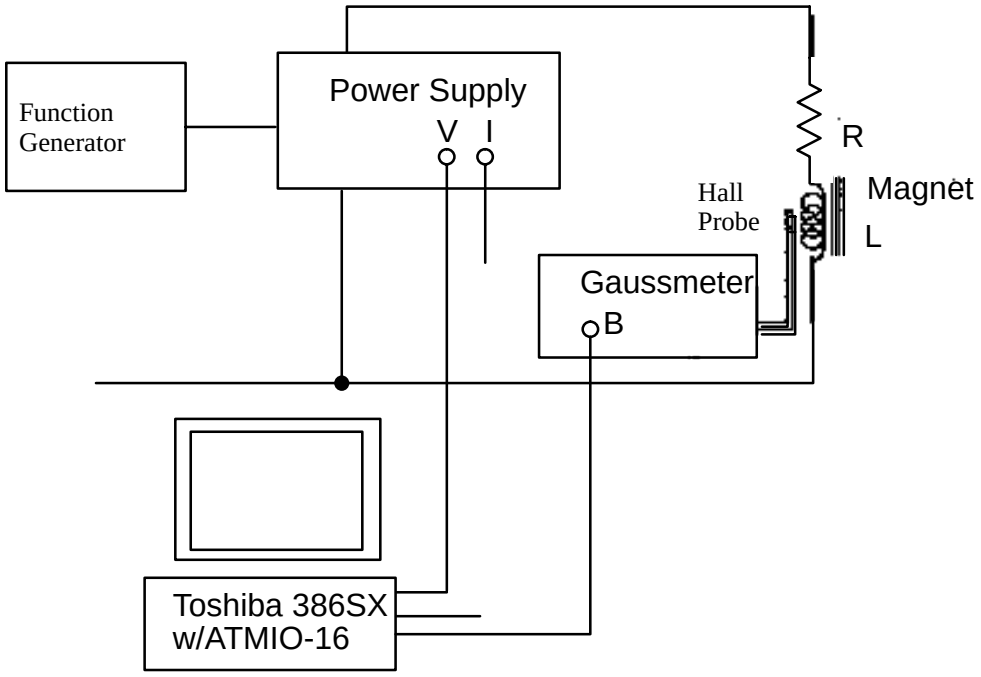

Fig. 5.1: Measurement setup for the eddy current effect on the magnet field. The voltage and the current signals are provided by the power supply and the magnet field is measured by a gaussmeter with a Hall probe. These analog signals are digitized by the ATMIO–16 board and analyzed by a computer.

The magnet field was measured using a Series 9900 menu–driven multi–channel gaussmeter manufactured by F.W. Bell. A three–axis Hall probe was used, and only one of the three channels was used for the measurement of the horizontal field. Due to the relative nature of this measurement, the Hall probe was placed approximately at the center of the magnet without much precision. The full–scale analog output signal level is ±3V.

The power supply was a Kepco bipolar operational power supply/amplifier, model No. BOP 20–20M, with a voltage range of ±20 V, maximum current of 20 A, and bandwidth of 4 kHz. It was put in voltage–controlled mode for this measurement. Analog voltage and current monitoring signals were provided through an interface card, and digitized and analyzed by a portable computer. The full–scale signals are ±10 V for both the voltage and the current.

The ATMIO–16 board, a multichannel DAC/ADC, has 16 input channels. Configured for differential input, as in our setup, the maximum number of channels is 8. The analog input signal range for the ATMIO–16 board is ±10 V for all channels. With the digital resolution of 12 bits, the conversion formula is

$$\text{V (in analog)} = \frac{10}{2,048}\text{V (in digital)}. \tag{5.1}$$

This gives a resolution of approximately 5 mV.

The data acquisition and analysis was done by a portable computer with a 386SX processor and a math coprocessor. The data was obtained for 20 periods with a total of 1000 data points. Given a nominal frequency supplied by the user, the actual frequency was first found by counting the integer number of periods and the time elapsed as measured using the clock on the ATMIO board. Using this frequency f, the data was fit to the function

$$V = V_0 \cos(2\pi ft + \phi) \tag{5.2}$$

using the linear least squares method,[2] which gives the amplitude V_0 and the phase ϕ. This procedure was done for the voltage, the current, and the magnet field, and the amplitudes and the phases were compared to obtain the resistance and the inductance of the magnet and the attenuation and the phase shift of the field due to the eddy current.

5.2 Measurements and Results

The analog–to–digital conversion was done at the maximum rate of 100 ksamples/sec, which introduces a timing error of 10 μsec between two adjacent channels. With sinusoidal signal of frequency f, the phase measurement error per Hz per channel is

$$\frac{\Delta\phi \text{ (degrees)}}{\text{f (Hz)}} = 3.6 \times 10^{-3}. \tag{5.3}$$

The result of measurement on $\Delta\phi$/f at the frequencies of 10, 100, and 200 Hz is shown in Table 5.1. This phase error was compensated for in the subsequent measurements.

Let us write

$$\frac{V_i}{I_i} = \left|\frac{V_i}{I_i}\right| e^{i\phi}, \tag{5.4}$$

which gives, using Eqs. (2.8) and (2.11),

$$R = \left|\frac{V_i}{I_i}\right| \cos\phi \qquad \text{and} \qquad L = \frac{1}{\omega}\left|\frac{V_i}{I_i}\right| \sin\phi\,. \tag{5.5}$$

The current I_i and the field B are related by

$$B = C\left|I_i\right| \, a e^{-i\varphi}, \tag{5.6}$$

Table 5.1: Measurement results of the phase delay between channels 1,2, and 3 of ATMIO–16 board.

Frequency (Hz)	**$\Delta\phi$/f (degrees/Hz) between Channels 1&2**	**$\Delta\phi$/f (degrees/Hz) between Channels 1&3**
10	–3.50E–03 ± 1.61E–04	–7.05E–03 ± 2.38E–04
100	–3.59E–03 ± 1.59E–05	–7.19E–03 ± 1.86E–05
200	–3.60E–03 ± 4.57E–06	–7.21E–03 ± 7.15E–06

where C is a factor that normalizes a to 1 at $\omega = 0$. a and φ are the attenuation factor and the phase shift in Eqs. (4.10), (4.11), and (4.12).

Since the resistance given in Eq. (5.4) includes the resistance of the coil winding R_c, we must subtract it from the measured resistance to obtain the resistance due to the eddy current R_e. To avoid the offset calibration error in the output monitoring signals provided by the power supply, we apply an AC signal of very low frequency, say 0.1 Hz rather than use a DC signal and measure the amplitude ratio. The result is

$$R_c = \left|\frac{V_i}{I_i}\right|_{f=0.1\ \mathrm{Hz}} = \frac{431\ \mathrm{mV}}{928\ \mathrm{mA}} = 0.464\Omega\ . \tag{5.7}$$

Measurement on the B field done simultaneously gave an estimate of the normalization factor C in Eq. (5.5). The result is

$$C = \left|\frac{B}{I_i}\right|_{f=0.1\ \mathrm{Hz}} = \frac{11.1\ \mathrm{G}}{928\ \mathrm{mA}} = 11.9\ \mathrm{G/A}. \tag{5.8}$$

Four sets (1, 2, 3, and 4) of measurements were made. For cases 1 and 4, either the voltage amplitude was maintained at ≈15 V or the current amplitude at ≈15 A, whichever was larger. At the maximum current of 20 A from the power supply, we will have about 240 G, and the scale on the gaussmeter was set to 300 G. On the other hand, for cases 2 and 3, the current was maintained at ≈1 A, which produced a magnetic field of ≈12 G. For these cases, the scale on the gaussmeter was set to 30 G. The plots of the variation of the input voltage and the input current are shown in Fig. 5.2.

In Figs. 5.3(a) and 5.3(b) are shown the results of measurements on the magnet field–current ratio $|B/I_i|$ and the phase shift for the vertical correction winding of the storage ring sextupole, and in Figs. 5.4(a) and 5.4(b) are shown the results of measurements on the resistance and the inductance of the same magnet. Five measurements were taken for each frequency, and the error bars shown indicate the standard deviation of the data.

The magnet field–current amplitude ratio $|B/I_i|$ shown in Fig. 5.3(a) is constant at 12 Gauss/A within ±0.6% and does not show any tendency to decrease. In case of the phase shift, the differences in the rate of decrease may be due to the hysteresis effect, which changes the μ, the instantaneous slope on the B–H curve, depending on the residual magnet field with the current turned off. With the phase delay in the range $-3.6° < \varphi < -2°$ at 200 Hz, we obtain from Eq. (4.13),

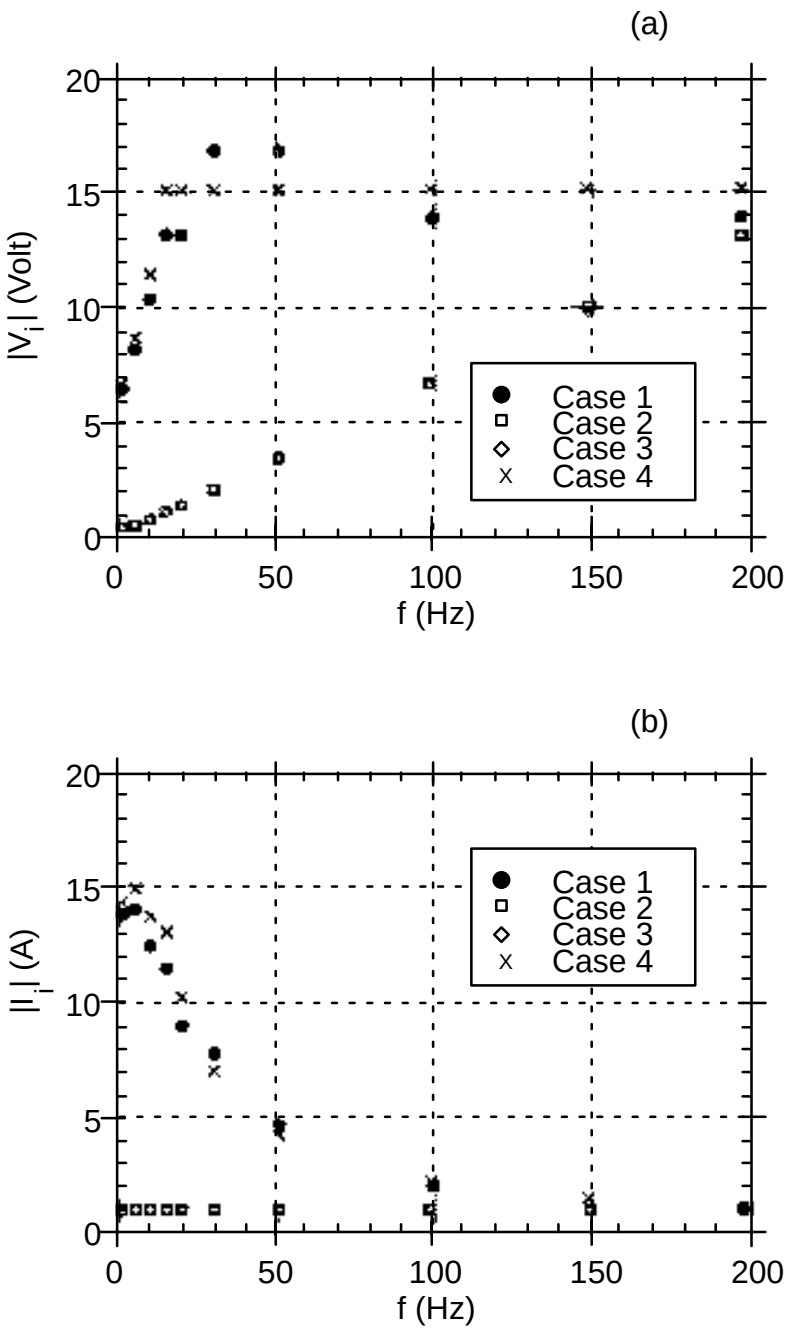

Fig. 5.2: Variation of (a) the input voltage amplitude $|V_i|$ and (b) the input current amplitude $|I_i|$ for different cases of measurements.

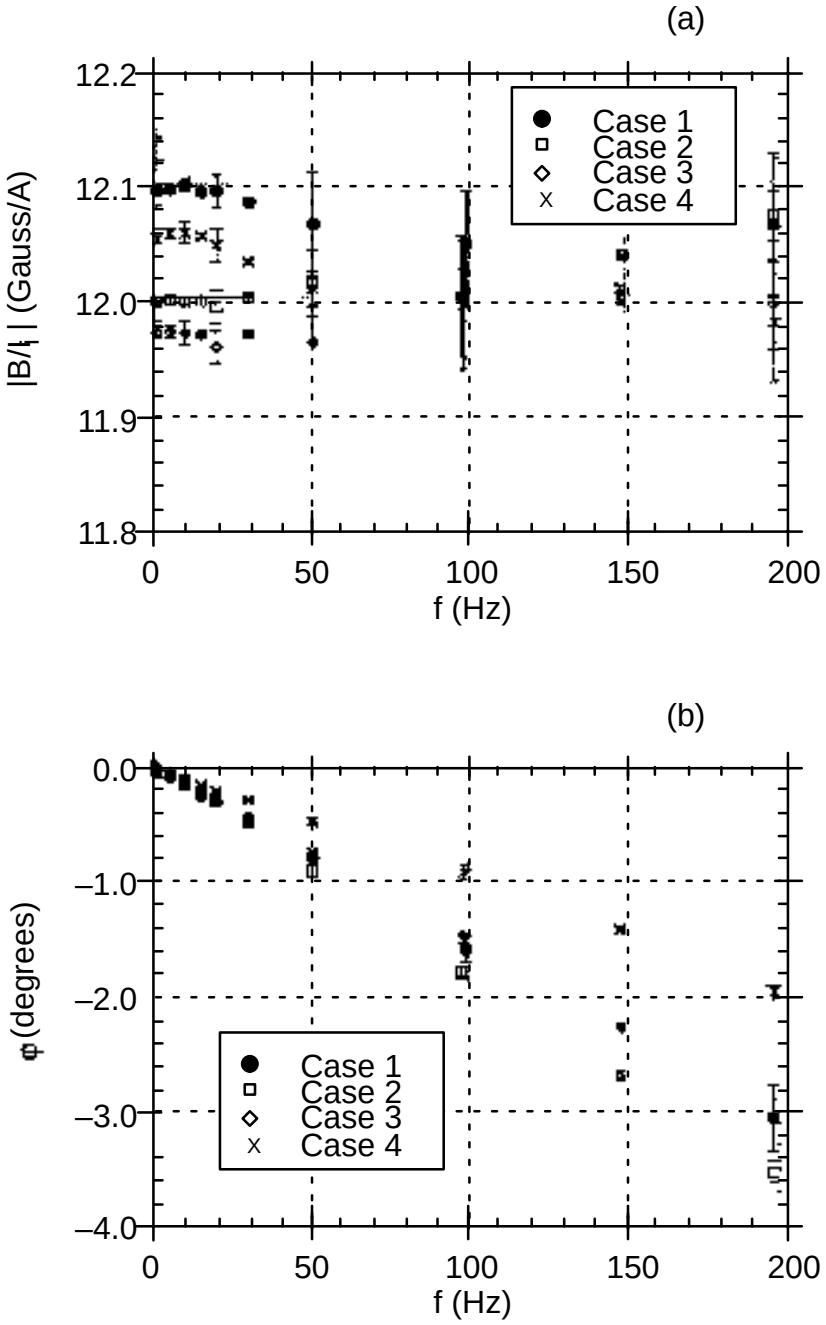

Fig. 5.3: Results of measurements on (a) magnet field–current amplitude ratio $|B/I_i|$ and (b) the phase shift φ.

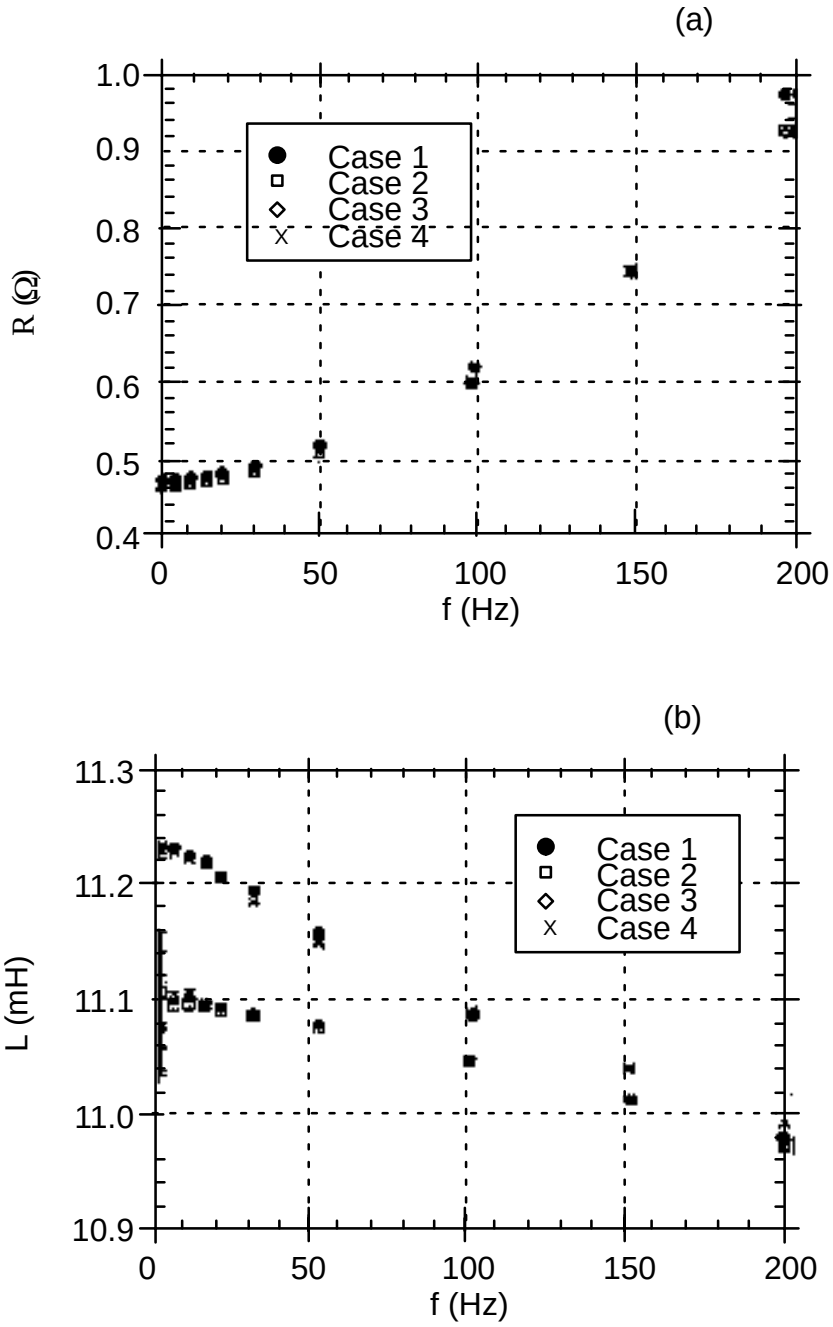

Fig. 5.4: (a) Result of measurements on the resistance R. The error range is within the marks. (b) Result of measurements on the inductance L. For cases 1 and 4, the error range is within the marks, and for cases 2 and 3, the error (±0.04 mH) is significant only at the lowest frequency of 1 Hz.

$$300 < K_m\left(=\frac{\mu}{\mu_0}\right) < 550\ . \tag{5.9}$$

Fitting the measurement data on the magnet resistance R shown in Fig. 5.4(a) with a quadratic function in frequency gives

$$R \approx 0.465 + 6.53 \times 10^{-5}\omega + 2.56 \times 10^{-7}\omega^2. \tag{5.10}$$

In Eq. (5.10), the first term represents the power loss in the coil winding, the second term is the hysteretic loss, and the third term is the loss due to the eddy current in the core.

The results of measurements on L presented in Fig. 5.4(b) show good agreement between cases 1 and 4 and between cases 2 and 3. These differences are attributed to changes in μ with field amplitudes. The decrease of L with increasing frequency, however, was found to be much larger than predicted. Assuming that V_{eff} is large enough so that Eq. (4.31) holds true within the frequency range of our interest, we have from Eq. (4.25) using Eq. (5.9)

$$1 - \frac{L_{ea}\ (f = 200\ Hz)}{L_{ea}\ (f = 0\ Hz)} = 8.5 \times 10^{-4}, \tag{5.11}$$

which is too small to explain the inductance decrease of 1% for cases 2 and 3 with constant current amplitudes. This indicates that some of magnetic flux has either disappeared or shifted from a dense region to a dilute region as frequency increased. This is because the fringe field previously ignored in the 2–D calculation, which was quite strong at low frequency, became very small at high frequency due to the eddy current. As shown in Fig. 5.5(a), when the frequency is low enough, there are field lines emanating from the side which is not laminated. However, as the frequency increases, eddy current develops in the direction that cancels the original field on the end side, while the field in the gap between the poles remains virtually unchanged, as shown in Fig. 5.5(b). This causes the effective volume V_{eff} to decrease, and thus from Eq. (4.24), the overall magnet inductance decreases. A preliminary measurement on the sextupole magnet showed that the field near the pole in the middle of the magnet bore was 3.5 kG and the field on the side of the pole was approximately 300 G with 200 A of current in the main coil winding of the sextupole magnet.

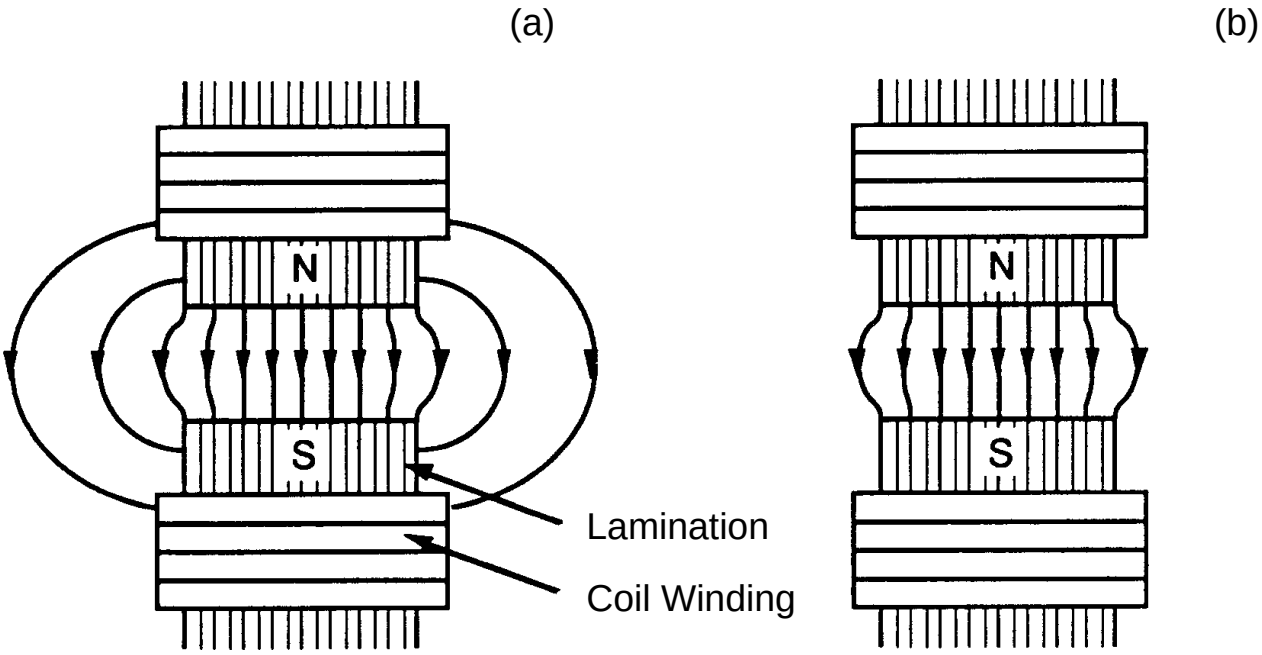

Fig. 5.5: Schematic comparison of the magnetic field between (a) at low frequency and (b) at high frequency when the eddy current cancels out the side field.

6. Summary and Conclusion

In the previous sections, theory and measurements of the effect of the eddy current in the laminations on the magnet field were presented. The theory assumes a simple solenoid–type magnet with laminated iron core and ignores the end field effect. The measurements were made on the input voltage and current, and the dipole component of the magnetic field in the middle of the magnet bore.

The focus of the study was on the frequency dependence of the field attenuation factor, the phase delay, and the resistance and inductance of the magnet. The results of measurements show good agreement with the theory. In the case of the magnet inductance, the one–dimensional nature of the theory resulted in a discrepancy between measurement and theory. This, however, could be explained by the eddy current induced by the longitudinal field on the end side of the magnet poles.

The measurements were done using a relatively small bipolar power supply with maximum voltage of ±20 V and maximum output current of ±20 A up to the frequency of 200 Hz. This set the limit on the current amplitude at 1 A and the magnetic field amplitude at ≈12 G. The design peak field at 7.0 GeV is 1.0 kG with the peak current of 103 A.[3] This difference of two orders of magnitude in the current capacity prohibited measurements over the full range of operation, which can be done only when the prototype power supplies for the corrector magnets become available.

Acknowledgment

G. Decker, K. Kim, and L. Turner are to be thanked for the helpful discussions on this work.

References

1. J. Jackson, *Classical Electrodynamics*, John Wiley & Sons, p. 241, 1975.
2. W. Press et al., *Numerical Recipes in C*, Cambridge University Press, p. 528, 1989.
3. APS Conceptual Design Report, Argonne National Laboratory, ANL–87–15, 1987.